MEMORANDUM
RM-3529-PR
JULY 1963

REVIEW OF PHYSICAL PROCESSES IN HYPERVELOCITY IMPACT AND PENETRATION

Robert L. Bjork

PREPARED FOR:
UNITED STATES AIR FORCE PROJECT RAND

The RAND Corporation
SANTA MONICA • CALIFORNIA

MEMORANDUM

RM-3529-PR

JULY 1963

REVIEW OF PHYSICAL PROCESSES IN HYPERVELOCITY IMPACT AND PENETRATION

Robert L. Bjork

This research is sponsored by the United States Air Force under Project RAND—contract No. AF 49(638)-700 monitored by the Directorate of Development Planning, Deputy Chief of Staff, Research and Development, Hq USAF. Views or conclusions contained in this Memorandum should not be interpreted as representing the official opinion or policy of the United States Air Force.

The RAND Corporation

1700 MAIN ST. • SANTA MONICA • CALIFORNIA

PREFACE

A continuing effort has been conducted on hypervelocity impact within RAND for several years. Applications of the results have been made to the problems of the meteoroid hazard, satellite vulnerability, and ICBM defense. This Memorandum presents some new information in this area and compares some of the earlier work with recent experimental data.

SUMMARY

The so-called volume-energy law, or two-thirds law, is an empirical fit which has been used by many writers to predict penetration by hypervelocity fragments. A comparison is drawn between this law and well-controlled high-velocity experimental results which have been obtained recently. The comparison reveals that the data fit the law satisfactorily at relatively low velocities but deviate from it in a marked way as impact velocities increase. It is therefore incorrect to extrapolate this law to predict impact effects in the meteor-velocity range.

The experimental data are shown to agree well with the author's earlier impact predictions based on a hydrodynamic model.* The agreement of penetration by aluminum spheres impacting 1100-F aluminum targets is particularly good. Penetration of the same spheres into 2024 alloy is less in all cases at corresponding velocities. It is observed that the ratio of the penetration in the two alloys increases with impact velocity, ranging from about 50 per cent at 3 km/sec to 75 per cent at 7.5 km/sec, which suggests that the relative importance of strength wanes with waxing velocity. The 25 per cent change in penetration occasioned by increasing the strength by a factor of 7.5 emphasizes the insensitivity to strength at high impact velocities.

Irreversible heating, accompanied by the creation of entropy, always occurs in a shock. Transit of the target by the shock system produced in hypervelocity impacts leaves the target material in a heated state. It is shown that impacts in the meteor-velocity range create enough heat by this mechanism to vaporize and liquefy portions

*Published in RAND P-1662, Effects of a Meteoroid Impact on Steel and Aluminum in Space.

of the target, while other portions are heated to a degree which drastically affects their strength. The temperature and physical state of the target material are presented as a function of depth for iron and aluminum targets struck by fragments of the same material at velocities of 5.5, 20, and 72 km/sec. The results indicate that target melting by this mechanism probably becomes the dominant physical process in determining crater size at velocities above about 20 km/sec. The results also reinforce the statements about the waning importance of material strength at high impact velocities. Although melting determines the crater size at high velocities, the model of Whipple based on target melting is shown to overestimate still the actual crater dimensions.

The physics of penetration of thin targets by hypervelocity fragments at an impact velocity of 20 km/sec is exemplified by detailed calculations of aluminum cylinders having length equal to diameter penetrating aluminum targets having thicknesses one-fifth and one-tenth the projectile length. The shock and rarefaction systems are followed and discussed. It is shown that the projectile is thoroughly shattered in these impacts, and that a spray of shattered projectile and target material emerges behind the perforated plate. Effects of the spray on a second target placed behind the first are discussed, and the hole size produced in plates of various thicknesses is estimated and presented graphically.

The question of whether or not the projectile material exerts an appreciable influence on the hypervelocity penetration process has been controversial. Previously, A. E. Olshaker and the author had

presented scaling laws to account for projectile-material influence on a shock-impedance model. Publications are cited which deny the existence of this effect. Comparisons are drawn between the two theoretical predictions and recent well-controlled experimental results. The effect of projectile material is unambiguously demonstrated, and excellent agreement with the shock-impedance law is found. The agreement is found to extend over a wide range of projectile materials, from copper and steel on the one hand to plastics having specific gravity less than unity on the other. It is concluded that by combining the shock-impedance law with the earlier predictions on the hydrodynamic model, the penetration by projectiles of any material into aluminum targets may be predicted up to velocities of about 20 km/sec. Above this impact velocity, the effects of melting and vaporization are expected to become important in establishing the crater dimensions. The role of projectile material in this physical regime has not been studied as yet.

CONTENTS

SYMBOLS

a = constant used in fit

B, BHN = Brinell hardness number

B-A = subscript indicating projectile of material B incident on target of material A

b = constant used in fit

D_h = hole diameter

d = projectile characteristic dimension

E = projectile kinetic energy

e = base of Naperian logarithms

F = normalized penetration ratio (defined on p. 40)

m = constant used as exponent

n = constant used as exponent

P = pressure

p = penetration

r = radial distance in cylindrical coordinate system

t = target thickness

u = particle velocity

V = crater volume

v = impact velocity

x = distance parallel to axis in cylindrical coordinate system

β = exponent in fit of penetration as a function of density

π = normalized penetration (p/d)

ρ_A, ρ_B = density of materials A and B, respectively

ρ_p = projectile density

ρ_t = target density

σ_o = material yield strength

I. CRATERING IN THICK TARGETS

VOLUME VERSUS ENERGY

The idea has been put forth by many writers that the volume of the crater produced in a thick target is proportional to the kinetic energy of the projectile which produced it. If one assumes also that the crater geometry remains similar throughout a region of the velocity spectrum, then the two assumptions taken together lead to the hypothesis that penetration is proportional to the two-thirds power of the impact velocity. In practice, both assumptions encounter difficulties.

For impacts between projectiles and targets of like materials, the similar-geometry assumption is usually well founded in the hypervelocity regime, the craters being approximately hemispherical. However, for impacts between unlike materials, substantial deviations from hemisphericity are observed, and the geometries do not remain similar as the impact velocity is changed. For example, iron or copper spheres striking aluminum targets at 2 or 3 km/sec produce craters whose depths are about equal to their diameter. At about 7 km/sec, these spheres yield craters whose depths are about 80 per cent of their diameters. The ratio for hemispherical craters would be 50 per cent.

Projectile geometry can also produce departures from hemisphericity, even for like-material collisions at very high velocities. For example, aluminum jet pellets impacting 2024 aluminum targets at 10 km/sec are found to produce craters whose depths are 80 per cent of their diameter.* The pellets have lengths about three times their

*Personal communication from J. Kineke.

diameter. The variation of crater geometry with impact velocity for this type of projectile has not been thoroughly investigated.

The assumption that crater volume is proportional to projectile kinetic energy encounters difficulty at any fixed velocity when one considers projectiles of various materials impacting on a given target material. More and more experimental data are accumulating which demonstrate that projectiles of the denser materials are more efficient in producing craters, in that they produce a greater crater volume per unit kinetic energy. If one wishes to take account of these experimental data and still retain the physical flavor of the "volume-proportional-to-kinetic-energy" hypothesis, he must choose a different constant of proportionality for each set of projectile and target materials. Several attempts have been made to fit the variation of the proportionality constant by correction factors of the form

$$p \sim \left(\frac{\rho_p}{\rho_t}\right)^n v^{2/3}$$

In such fits, n is an empirically determined constant. In Ref. 1, we propose a physical basis for the success of such density corrections, but it is shown there that n has a slight velocity dependence. Of course, the $v^{2/3}$ dependence is an empirical fit which is valid only over a limited portion of the velocity spectrum.

Examination of log-log plots of penetration versus impact velocity reveals the power of velocity on which the penetration depends. The power is given by the slope of such plot. Typical plots show a linear dependence of penetration on velocity at low velocities. The slope of the curves generally decreases with waxing velocity, and for

many metals becomes approximately 2/3 in the velocity range of 3 to 5 km/sec. This velocity range has been extensively investigated in the last few years, and the 2/3 value of the slope has been cited as substantiating evidence for the volume-energy law. Such arguments ignore the difficulties cited above.

Experimental data have recently been accumulated in the velocity range of about 6 to 9 km/sec. These data quite clearly demonstrate that the penetration increases with a power of velocity less than 2/3. In addition, actual measurement of the crater volumes indicates that they increase less than linearly with projectile kinetic energy.

It should be emphasized that the "two-thirds law" is only an empirical fit. No defensible physical theory has been set forth to support it. An early attempt in this direction was made by Whipple, who proposed that the kinetic energy of the projectile was used to melt the material in the crater as well as the projectile. Under this assumption, all the material in the crater receives exactly enough internal energy to melt it, and the volume of the melted material is thus proportional to the kinetic energy of the projectile. However, the physical understanding which we now have of the process indicates that the average internal energy imparted to the crater material increases with impact velocity. Thus, to assume that the projectile energy goes almost entirely into heating would lead to the prediction that the penetration increases with a power of the velocity which was less than two-thirds. Moreover, Whipple's theory does not explain the pronounced effect of projectile density on the crater dimension.

Another notion proposed was that in expanding, the crater did work against a yield strength, σ_o, of the metal being deformed. Thus, the work done in forming the crater is $V\sigma_o$, this work being supplied by the projectile's kinetic energy. Under this model, the constant of proportionality between kinetic energy and volume is just σ_o, which should be a characteristic of the target material only. Again, the dependence of crater dimension on projectile material is not explained.

Despite the difficulties which the volume-energy law encounters in the lower-velocity range, and its lack of theoretical justification, it has become common practice for writers to extrapolate the law to cover the meteor-velocity range of 11 to 72 km/sec. The practice has become so common that a worker in another field who surveys the literature is liable to accept the validity of the extrapolated volume-energy relation only on the basis of the number of writers who have made this extrapolation.

Recent carefully controlled experiments at the higher velocities have been conducted which demonstrate that the volume-energy law is not being followed. For each combination of projectile-target materials, it is found that the volume increases more slowly than the energy, with the result that the ratio, V/E, decreases as impact velocity rises. Some examples will be given to illustrate this fact.

For the purpose of drawing comparisons, we will consider the penetration law recently proposed by Eichelberger and Gehring,[2] which states that in thick target impacts, hemispherical craters will be formed for which

$$V = 4 \times 10^{-9} \frac{E}{B} \qquad (1)$$

where V is the crater volume in cubic centimeters, E, the projectile kinetic energy in ergs, and B, the Brinell hardness number of the target material in kilograms per square millimeter. This relation is asserted to be valid over the meteor-velocity range and to hold for projectiles of any material.

Figure 1 shows the values predicted by Eq. (1) for penetration of aluminum projectiles into the 1100-F alloy of aluminum, compared with experimental results. The experiments were conducted by Atkins[3] and Liles and Goodman[4]. Both sets of experiments utilized spherical projectiles fired from light-gas guns, and the projectiles were fired in sabots to prevent erosion in the gun barrel. Liles and Goodman reported the Brinell hardness numbers of their targets to lie in the range of 15.9 to 17.8 kg/mm^2. The average value of 16.85 was used in evaluating Eq. (1) in order to plot it in Fig. 1. The prediction of the author, which was calculated on a hydrodynamic model,[5] is shown as the shaded region in Fig. 1.

At the lower experimental velocities, Eichelberger and Gehring obtain good agreement with the data. However, above about 5 km/sec the experimental results deviate from their prediction. The reason for the deviation becomes evident if we consider the variation of the energy-volume ratio as a function of impact velocity. This is plotted in Fig. 2. Liles and Goodman[4] measured the crater volumes individually by accurately metering a liquid into them. Eichelberger and Gehring predict a constant V/E ratio of 2.42×10^{-10} cc/erg, whereas the midpoint of the experimental data goes from about 1.8×10^{-10} at 3 km/sec to about 1.1×10^{-10} at 7.5 km/sec.

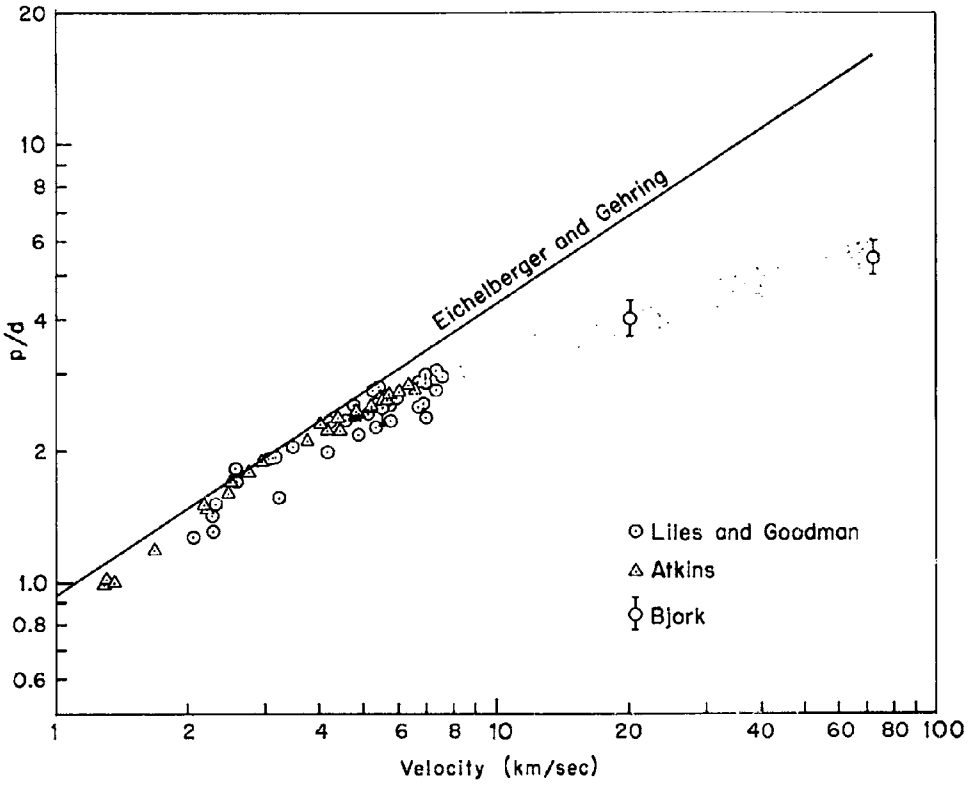

Fig. 1 — Penetration of aluminum projectiles into 1100-F aluminum targets (The theoretical point at 5.5 km/sec is nearly obscured by the experimental data)

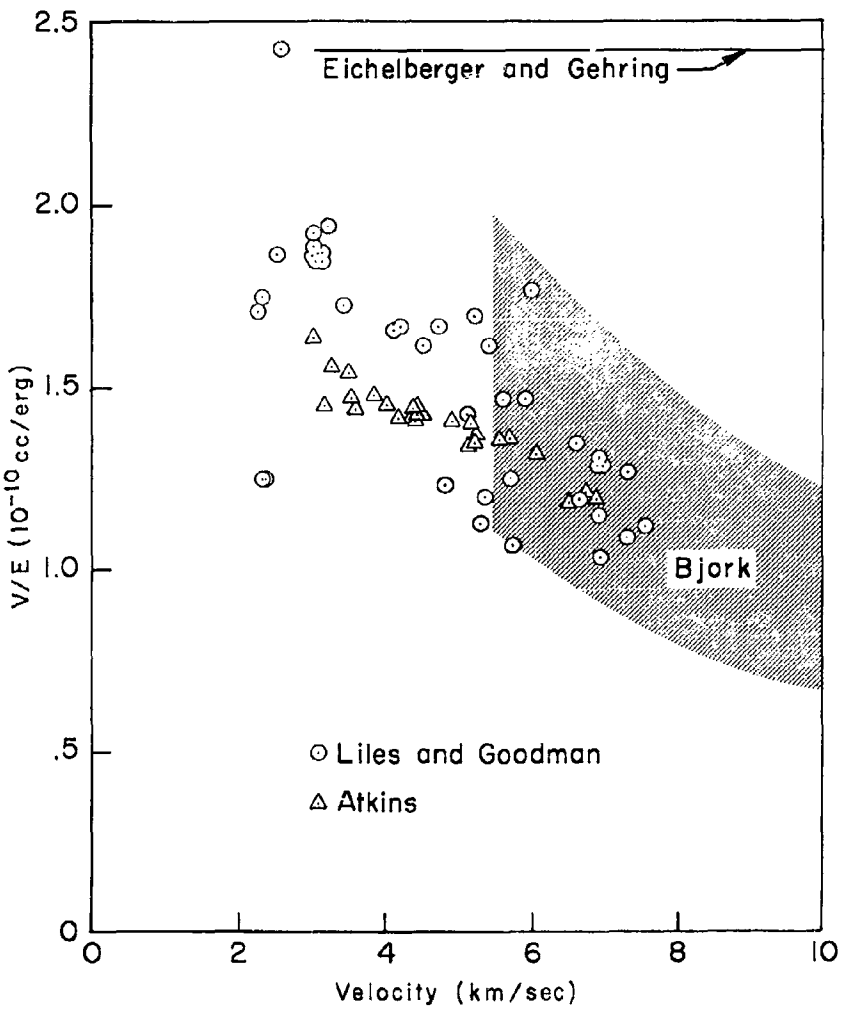

Fig. 2— Ratio of crater volume to projectile kinetic energy as a function of impact velocity for aluminum spheres on 1100F aluminum targets

The values of V/E measured by Liles and Goodman[4] for copper spheres impacting on 1100-F aluminum targets are shown in Fig. 3 as functions of impact velocity.* The values are notably higher than for aluminum projectiles, running from about 2.6×10^{-10} cc/erg at 3 km/sec to about 1.9×10^{-10} at 6.5 km/sec. The model of Eichelberger and Gehring, which does not differentiate among projectile materials, still predicts the constant value of 2.42×10^{-10} cc/erg. For this particular combination of projectile and target materials, Eichelberger and Gehring obtain fair agreement at the lower impact velocities but again depart seriously from experiment as the experimental values of V/E decrease with velocity.

For completeness, the volume-energy ratio found by Liles and Goodman[4] for copper targets is plotted in Fig. 4 as a function of velocity.* In this case also, the volume-energy ratio is found to decrease with velocity, and the ratio for copper projectiles is substantially higher than that for aluminum projectiles at the same velocity.

For these targets, which have Brinell hardness numbers ranging from 48.9 to 50.9, the equation of Eichelberger and Gehring predicts a constant V/E of 0.802×10^{-10} for both projectile materials. Their prediction is plotted in Fig. 4 as the flat line. Besides failing to make the important distinction between projectile materials, their prediction departs seriously from the experimental results as the impact velocity increases.

---

*The straight lines bracketing the data groups in Figs. 3 and 4 have been inserted only to illustrate the data trend. They should not be extrapolated.

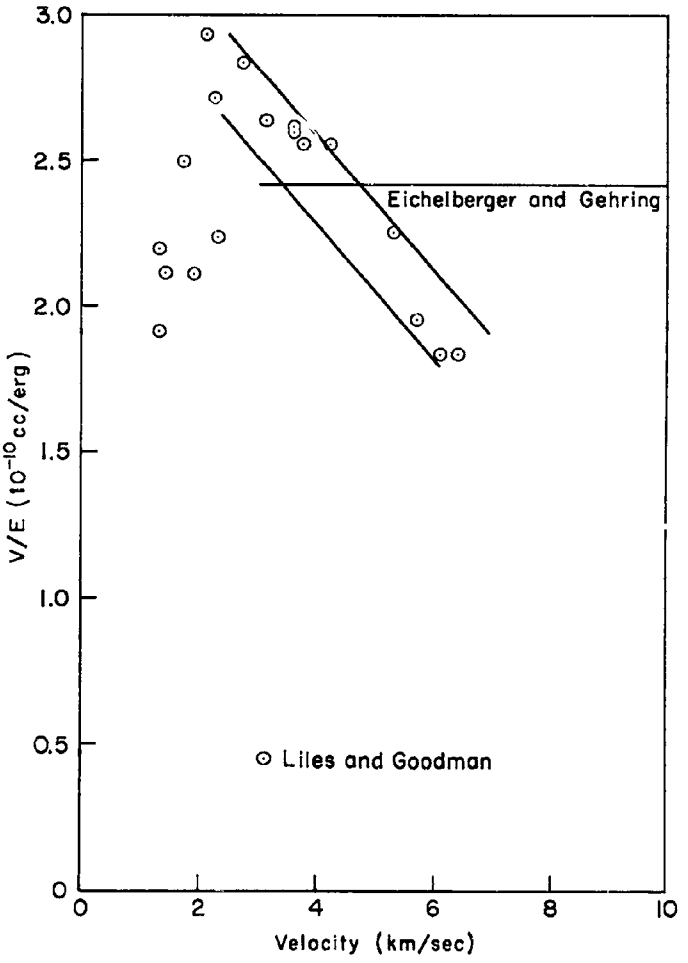

Fig. 3—Ratio of crater volume to projectile kinetic energy as a function of impact velocity for copper spheres on 1100-F aluminum targets

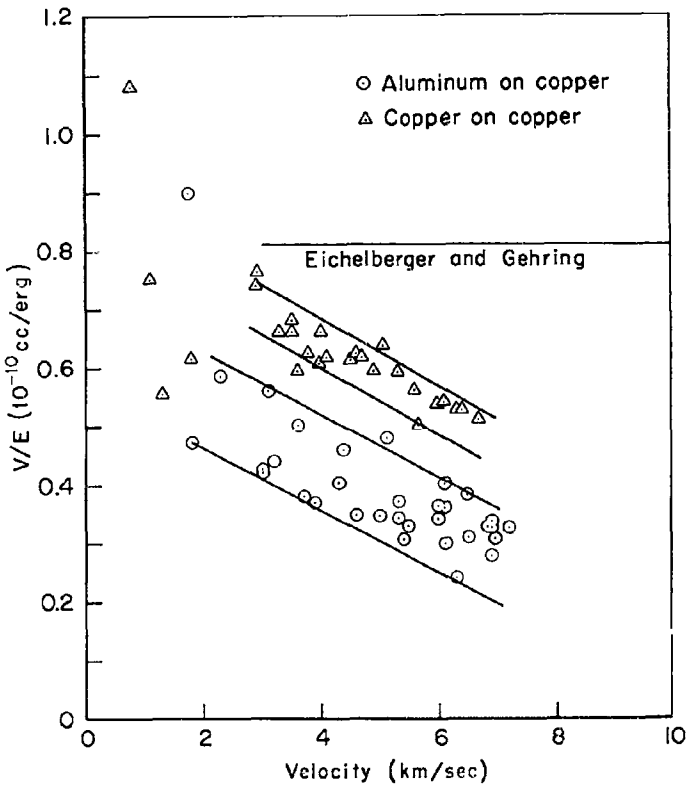

Fig. 4—Ratio of crater volume to projectile kinetic energy as a function of impact velocity for aluminum and copper spheres on copper targets (Data due to Liles and Goodman [4])

The hypothesis that crater volume is directly proportional to projectile kinetic energy rests solely on empirical grounds. In the lower velocity range, where the hypothesis holds fairly well, the constant of proportionality is a function of both the projectile and target materials. There is no theoretical justification for extrapolating the relation outside the regime where the empirical fit was obtained. Indeed, for copper and 1100-F aluminum targets, where well-controlled experimental data at very high impact velocities exist, the hypothesis of constant volume-energy ratio is found to be incorrect.

HYDRODYNAMIC PENETRATION

Penetration of aluminum projectiles into aluminum targets at velocities of 5.5, 20, and 72 km/sec were calculated on the hydrodynamic model and published by the author in 1958.[5] The projectile geometry considered in these calculations was that of a square cylinder (length equal to diameter), which moved along its axis of symmetry. The results are plotted as the shaded region in Fig. 1. The ordinate in this figure is the normalized penetration, p/d, where p is the penetration depth and d is the length of the projectile.

Since no other projectile geometries have been treated theoretically, one must examine experimental data to determine how to apply the theory to other projectile shapes.

A way of comparing the penetrations of spheres and square cylinders was suggested by Collins and Kinard[6] based on their experiments with both types of projectiles. For a given set of projectile-target materials they found that the penetration depended only on the projectile length, rather than on the projectile mass. Choosing the cylinder

length (which equals its diameter) and the sphere diameter as characteristic dimensions, d, led to plots of p/d versus impact velocity which were identical for their data. The surprising conclusion is that a sphere of given diameter produces the same penetration as a square cylinder which has the same characteristic dimension, but which weighs 50 per cent more. Their data included cases of aluminum-on-aluminum impacts.

A possible criticism of their data is that it was apparently taken with unsaboted projectiles, and that aluminum projectiles have been found to lose a substantial fraction of their mass by erosion during flight through the launch tube.

On the other hand, Halperson and Atkins have presented data taken with aluminum spheres and cylinders fired in sabots.(7) For penetrations into the 1100-F aluminum alloy, their conclusion is that at a given impact velocity, the crater volume per unit projectile mass is the same for both geometries. The projectile masses were reported as 1.27 gm, but the dimensions of neither the cylinder nor its crater were specified. For this reason, one cannot be certain whether their result is in agreement with Collins and Kinard or not. Any disagreement is likely to be on the order of 10 per cent in penetration, which is comparable with the theoretical uncertainty and the scatter in even the best experiments, as illustrated in Fig. 1.

For irregular geometries, where one dimension greatly exceeds another, it is difficult to assign a characteristic dimension. In this case, some success has been obtained by choosing the equivalent sphere diameter as the characteristic dimension, i.e., the diameter of the sphere having the same mass as the projectile. In Section IV

we will show that this yields a satisfactory treatment of flat disks, for example, the steel disks accelerated by the Ballistic Research Laboratories (BRL) explosive accelerator, and the plastic disks fired by the Ames Research Center light-gas gun.

However, even this treatment breaks down for the case of short, oriented rods. To exemplify this, the jet pellets fired by BRL at 10 km/sec have a length about 3 times their diameter and strike the target oriented end-on. The normalized penetration calculated using the equivalent sphere diameter greatly exceeds that expected from spherical projectiles striking at the same speed. The craters produced by the jet pellets are deeper and narrower than hemispherical, which is probably the source of the difficulty. However, they are not deep and narrow enough to be treated on the basis of shaped-charge jet theory. It is felt that more theoretical work is necessary in order to explain the penetration of short, oriented rods.

The theoretical craters were felt to contain a possible error of ± 10 per cent, which is denoted by the height of the shaded region. The portion of the theoretical craters below the original target surface was observed to be hemispherical within the limit of the error. It was also noted that the three calculated points could be fitted within the limits of the error by a curve having the form

$$\frac{p}{d} \sim v^{1/3}$$

In view of the fact that the fastest experimental shots at that time lay in the range of 15,000 to 17,000 ft/sec (and there were very few of these), and that the experimental results differed among themselves

by a factor of two or more, the error cited seemed small indeed, and a more refined fit did not seem justified. However, the excellent agreement of the theoretical points with recent experimental data, which extends into the velocity range treated theoretically, justifies a more careful treatment. Accordingly, the theoretical points are connected in Fig. 1, and in the following figures of the same type, by a smooth curve.

The equation of the curve is

$$\frac{p}{d} = 11.02 \exp\left\{\frac{-2.457}{v^{0.295}}\right\} \qquad (2)$$

where v, the impact velocity, is given in km/sec. The form of the fit was chosen to produce a smooth change of curvature on a log-log plot of p/d versus v. It is noteworthy that this fit agrees with both the magnitude and slope of the experimental data. For a given value of velocity, the possible error in p/d should still be taken to be 10 per cent. For 1100-F targets, it is believed that this equation will be accurate to within the limits of error prescribed for the velocity range of 5.5 to 20 km/sec. At lower velocities, the equation will overestimate the penetration because of material-strength effects which the hydrodynamic model does not consider. At higher velocities, for reasons discussed in the section on melting and vaporization, the equation will underestimate the penetration. It is anticipated that penetrations will be about 40 per cent higher than predicted by the equation at impact velocities of 72 km/sec.

Assuming that the craters are hemispherical and employing Eq.

(2) leads one to the relation

$$\frac{V}{E} = \frac{3969}{v^2} \exp\left\{\frac{-7.371}{v^{0.295}}\right\} \qquad (3)$$

for the volume-energy ratio. Since the equation for p/d is cubed to obtain this expression, the limits of error are now ± 33 per cent. The shaded region in Fig. 2 shows the volume-energy ratio specified by Eq. (3). All the experimental points are encompassed by the theoretical region. Despite the large uncertainty, it is clear that a substantial reduction in V/E with increasing velocity is predicted and verified by the experimental data.

STRENGTH EFFECTS

Since the hydrodynamic model neglects material strength, the question naturally arises as to how well it simulates the actual physical process of an impact in a metal. Most investigators feel intuitively that the material strength must play an essential role in determining crater size.

In order to gain an insight into this question, we may consider penetrations into the various alloys of aluminum. These alloys are interesting in that they have essentially the same elastic properties, such as Young's modulus, sound velocity, and bulk modulus, but widely varying strength parameters. For example, the Brinell hardness number of the 1100-F alloy (commercially pure aluminum) is about 16, whereas the BHN for the 2024-T3 alloy is about 7.5 times as large, or 120.

In Fig. 5, the penetration of aluminum spheres in the two alloys

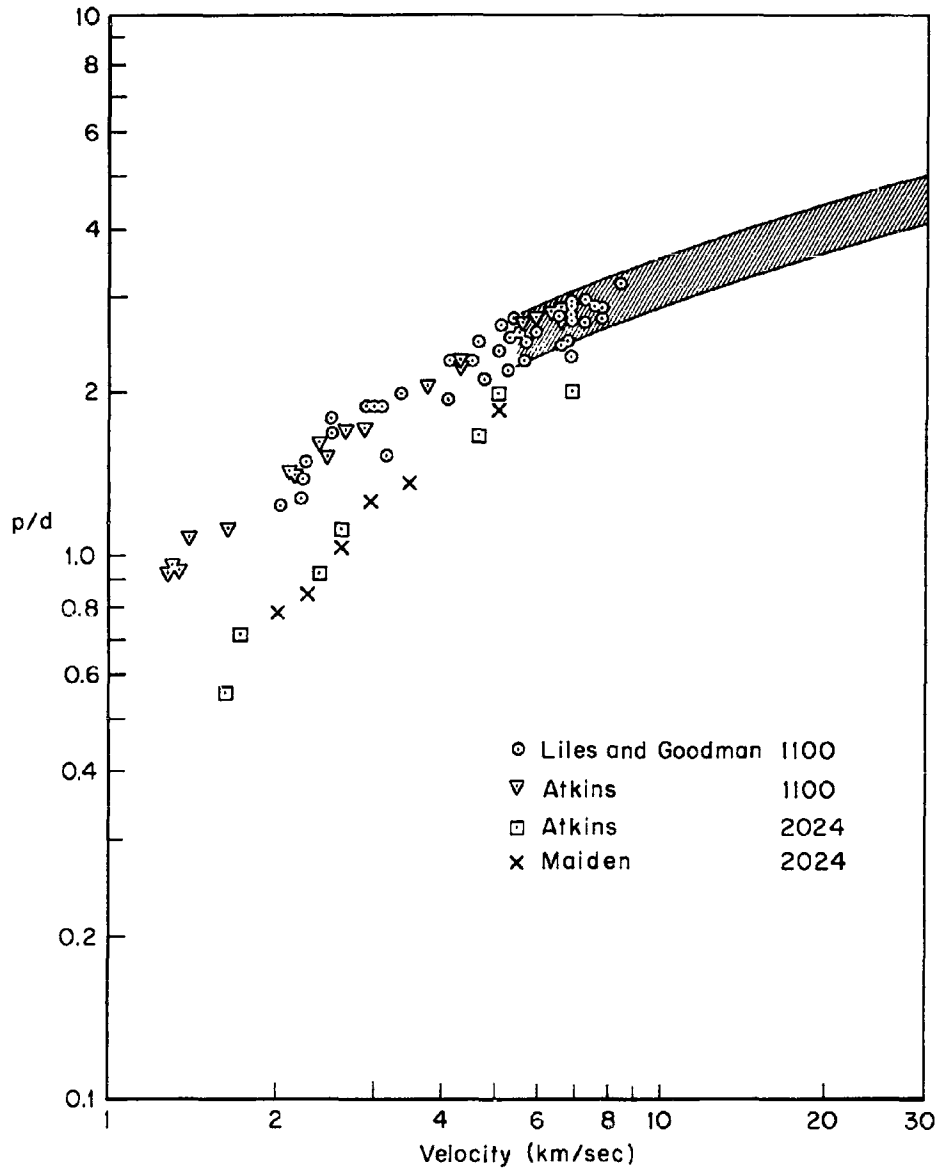

Fig. 5 — Normalized penetration (p/d) as a function of impact velocity for aluminum projectiles into 1100-F and 2024-T3 aluminum targets

is compared. At low velocities the penetration in 2024-T3 is about 50 per cent of that in 1100-F. At 7.5 km/sec the ratio has increased to 74 per cent. These experimental results strongly suggest that the ratio of penetrations in the two alloys is drawing closer to unity as the impact velocity is increased. The theoretical considerations on target melting discussed in Section III indicate that at 20 km/sec and above the ratio will be essentially unity.

The experimental penetrations in the low-strength 1100-F alloy are seen to be in excellent agreement with those predicted by the hydrodynamic model[5] which is shown as the shaded region.

Since the two alloys are identical in almost all respects except strength, the reduced penetration in 2024-T3 must be ascribed to a strength effect. At the present time no satisfactory theory exists to calculate the penetration reduction due to material strength. We will discuss two considerations which suggest that the formulation of such a theory will be extremely difficult.

First, the penetration is already very insensitive to strength at 7.5 km/sec, an increase of BHN by a factor of 7.5 causing a reduction of only 26 per cent in penetration. If one sought to fit the penetration in various alloys by a factor involving some power of BHN, e.g.

$$p/d \sim (BHN)^m$$

or by linear interpolation

$$p/d \sim a + b(BHN)$$

he would obtain nearly the same result because of the insensitivity.

Moreover, if he chose any other strength parameter, e.g., shear strength or tensile strength, he could obtain nearly the same results, since the various strength parameters correlate quite well among themselves. Therefore, it is anticipated that experimental data will not distinguish definitively among the various strength parameters and their functional relation to penetration reductions.

A more basic difficulty arises from the fact that the final stages of crater formation occur in target material which has been conditioned by the initial shock.[8] At least one physical parameter is definitely known to be altered by this conditioning, namely, the temperature. One can easily imagine that others might be also, in view of the severe compression and re-expansion which the material has suffered. Thus the notion of using a normal-temperature strength parameter to scale high-velocity penetration is open to serious question. The parameter modification by shock-conditioning must be taken into account.

With the experimental results before us, however, it is probably safe to scale over the small penetration range by an expression of the form

$$p/d = 2.75 \left\{ \frac{16}{BHN} \right\}^{0.15}$$

which may be expected to predict penetrations in the various aluminum alloys at 7.5 km/sec.

II. MELTING AND VAPORIZATION

SHOCK HEATING AS A FUNCTION OF PARTICLE VELOCITY

When a hypervelocity projectile encounters a target surface, it generates a shock wave in the target. The shock propagates into the target material with supersonic velocity and is the first physical manifestation of impact which any element of the target feels. The shock's passage sets the target material into motion and heats it. In view of the creation of entropy in the shock front, the target material is left heated even after expanding back to zero pressure. Figure 6 shows the temperatures produced in four metals as a function of shock pressure. The numbers plotted in the figure pertain to material that is initially at zero pressure, is acted upon by a single shock of maximum pressure P, and then expands adiabatically back to zero pressure. The temperature after release is plotted as a function of the peak pressure.

For a given material, the pressure behind a shock may be expressed as a function of only the change in particle velocity across the shock. (Particle velocity is defined as the velocity of each material element.) In hypervelocity impact, it is common to consider the target as being at rest, so that the peak pressure may be expressed as a function of only the particle velocity behind the shock. In that case the release temperature may also be expressed as a function of particle velocity only. This is done for aluminum in Fig. 7, where the left ordinate scale gives particle velocity in km/sec, and the right ordinate scale gives the release temperature as well as the state to which the material reverts.

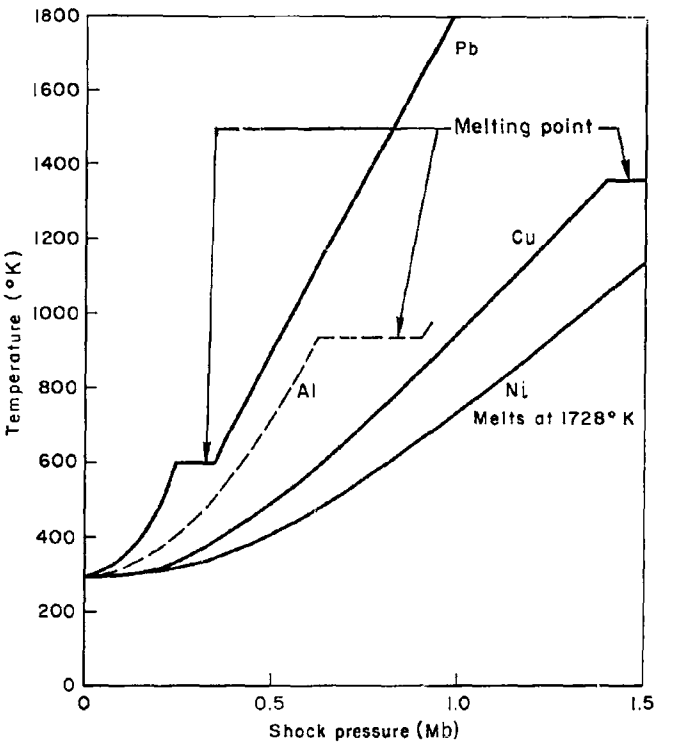

Fig. 6 — Release temperature as a function of shock pressure for four metals

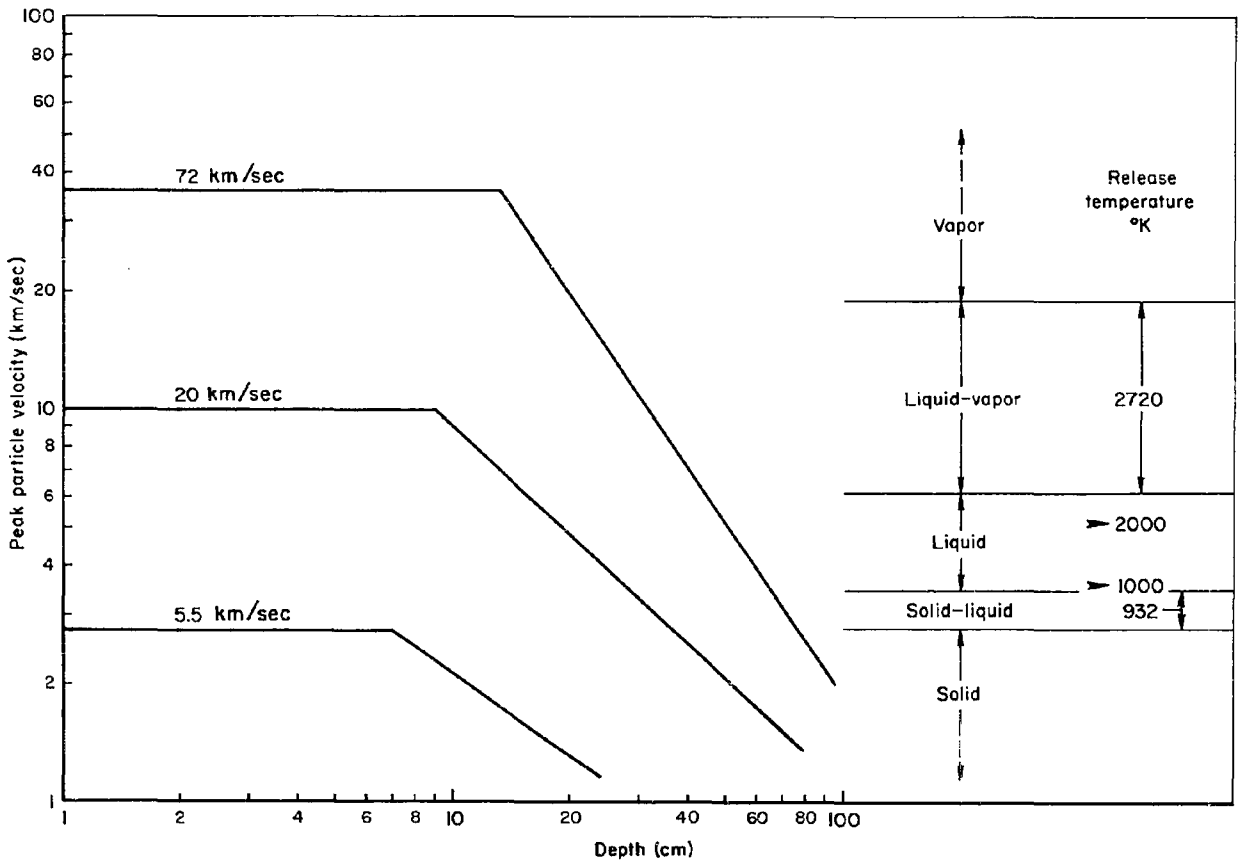

Fig. 7—Left scale: peak particle velocity as a function of depth along axis of symmetry for 10 x 10-cm aluminum cylinders striking end-on on semi-infinite aluminum targets
Right scale: release temperature and material state for same cases

The curves in Fig. 7 show the peak particle velocity as a function of depth along the axis of symmetry as calculated in Ref. 5. The curves in the figure are indexed by the impact velocity. Since these calculations referred to the impact of aluminum projectiles on aluminum targets, the initial particle velocity is half the impact velocity. Thus, the curve pertaining to an impact at 72 km/sec shows a particle velocity of 36 km/sec for small depths. Because the solution along the axis remains one-dimensional in nature until rarefaction waves from the target surface reach the axis, the curves all remain flat for a considerable depth. After this point, the peak particle velocity decreases with depth. Either the particle velocity or the release temperature may be read from the graph as a function of depth.

EFFECT OF TARGET MELTING ON CRATER SIZE

For the impact at 20 km/sec, it may be seen that the target material is melted to nearly the crater depth of 40 cm predicted purely on the basis of hydrodynamic flow. Thus, at about this impact velocity, one may expect that craters in all alloys of aluminum will have about the same depth, since the material strength does not influence the shock to a measurable degree at depths of less than 40 cm, and the melting characteristics of the various commercial alloys are similar. At impact velocities greater than 20 km/sec, the melted region will extend below the predicted craters. For example, at 72 km/sec the melted region is seen to extend to about 78 cm, which may be compared with the 55-cm penetration predicted in Ref. 5.

The numbers quoted should be considered preliminary estimates, which might be revised when a more thorough investigation is conducted. To reflect this fact, the estimated crater depth is shown as a dashed line in Figs. 18 and 19. However, it is possible to make some observations on the physics of the cratering process with more certainty. At impact velocities above 20 km/sec, the crater dimensions are determined essentially by the extent of the melted region. The fact that a new physical mechanism becomes important at higher velocities stands in contrast with the belief of Eichelberger and Gehring[2] that the physical mechanisms they considered were the only important ones over the meteoric-velocity regime.

The notion that material melting determines the crater size is strongly reminiscent of Whipple's hypothesis discussed in Section I, and the question logically arises as to whether Whipple might be correct for high velocities. The answer to this question comes from an examination of Fig. 7. Consider the case of an impact at 72 km/sec. The melted zone extends to about 78 cm, which we estimate to be the depth of the crater. However, the graph shows that the target material is completely vaporized to a depth of about 20 cm, is a mixture of liquid and vapor at a temperature of 2720°K to a depth of 45 cm, is liquid at a temperature substantially above the melting point down to about 66 cm, and is a mixture of liquid and solid at 932°K down to the final crater depth. In short, the average specific internal energy to which the crater material finally reverts is much greater than the heat of fusion. In addition, energy is delivered to other sources, e.g., kinetic energy and heating the material outside the crater.

Thus, a consideration of the energetics of the process indicates that Whipple must considerably overestimate the crater at the higher velocities.

Although the depths delineating the various state regimes may be slightly revised in the future, the qualitative physical observations are still expected to apply.

For impacts at velocities below 20 km/sec, the initial shock heating reduces the material strength and enhances the validity of the hydrodynamic model used in calculating the crater sizes. The reduction in strength may be expected to bring the craters in 1100 and 2024 alloys into closer and closer correspondence as the impact velocity is increased.

III. PHYSICS OF THIN-TARGET PENETRATION

Calculations based on the hydrodynamic model were made for aluminum cylinders striking aluminum plates at a velocity of 20 km/sec. The cylinder was chosen to be 10 cm long and 10 cm in diameter. Two target thicknesses were considered, namely, 1 and 2 cm. Although specific dimensions are prescribed in these examples, the problem is scalable, so that only the ratios of the dimensions are physically significant. Thus the results correctly describe the process where a square (length equals diameter) cylinder impacts targets whose thicknesses are one-tenth and one-fifth its length.

Figure 8 illustrates conditions 2.56 μsec after initial impact. In this figure and the following similar ones the x-axis is the axis of cylindrical symmetry, so that the target plate is depicted by the two parallel lines, x = o and x = 2 cm. An arrow in the figures denotes the particle velocity at the arrow's tail. The dashed line is the interface between projectile and target material. Pressure contours for the pressure values of 0.1, 1, 2, and 3 megabars are also shown.

Upon impact, two shocks are created, one moving into the target material and one moving upstream in the projectile material. For this particular set of conditions the shock moves upstream at about the same rate that the projectile moves forward, with the result that the shock remains nearly stationary relative to the target. In other words, the shock moves backward at about 20 km/sec relative to the projectile material, and the projectile material moves forward at 20 km/sec until it encounters the shock.

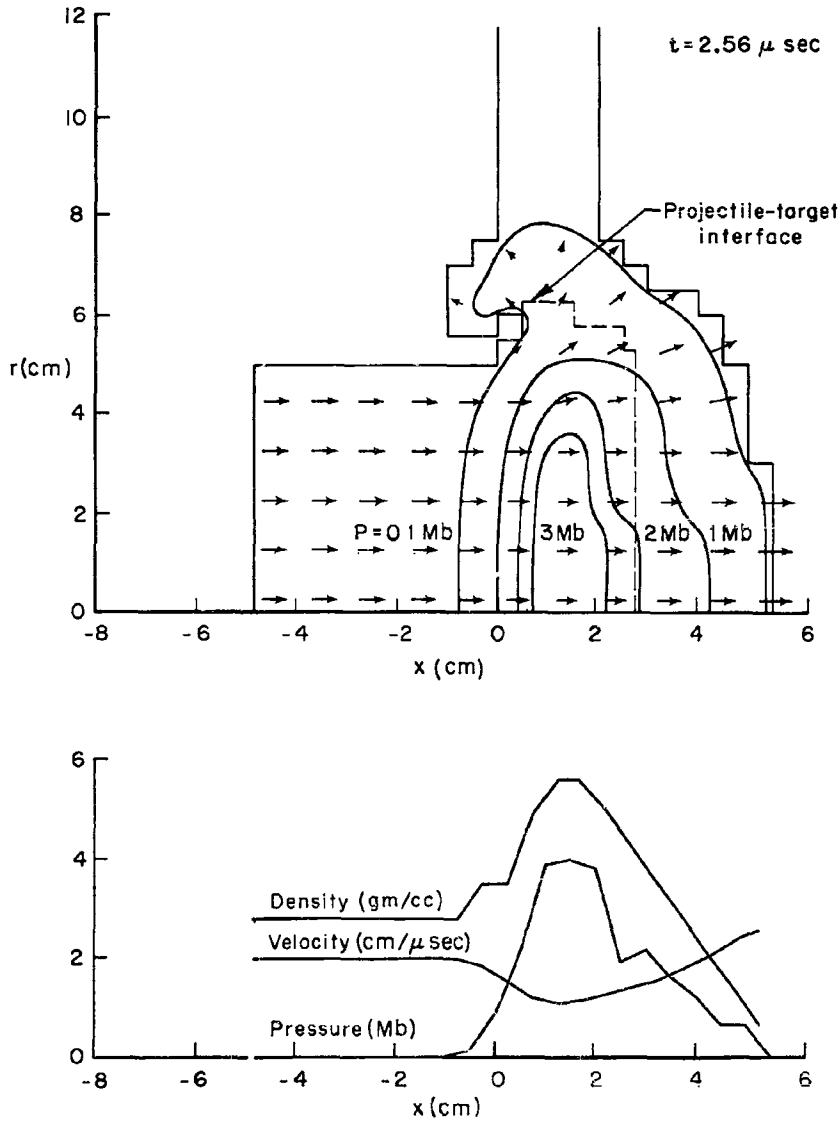

Fig. 8 — Aluminum cylinder (10-cm diameter, 10-cm length) striking 2-cm aluminum plate at 20-km/sec. Conditions: 2.56 μ sec after initial contact

The bottom half of Fig. 8 illustrates conditions along the axis of symmetry at this time. It may be seen that the projectile material moves unimpeded at a velocity of 20 km/sec until it reaches the left shock. In these calculations, the shock is purposely smeared out somewhat. The smearing is necessary in order that the numerical equations used be stable. In the actual impact, the shock would represent a discontinuity in velocity, pressure, and density at about $x = 0$, whereas the figure illustrates that these variables undergo a rapid, but continuous, change between about $x = -1$ and $x = 1$. On crossing the shock front, the material velocity is reduced to 10 km/sec, the density is raised to about 5.6 gm/cc, and the pressure is raised to about 5 megabars.

At the time of 2.56 μsec represented in the figure, the shock moving into the target has encountered the rear target surface and blown it off. As a result, a rarefaction wave moves into the shocked material. As may be seen, the material velocity increases smoothly in the rarefaction wave, and the pressure and density undergo a smooth decrease to zero values. The smooth variation corresponds to physical reality in this case. Reference to Fig. 7 shows that the shock is sufficiently strong to partly vaporize the target material. The material in the rarefaction wave will thus consist of a mixture of aluminum vapor and molten droplets, so that the pressure and density in the rarefaction must decrease smoothly in manner illustrated.

As the process progresses, the rarefaction wave will overtake the left shock and decrease its strength. That is, we may expect to see smaller peak pressures behind the left shock, we may expect to see a

smaller velocity drop as projectile material crosses the shock, and we may expect to see smaller densities. In effect, a race is occurring between the shock and the rarefaction overtaking it. If the shock maintains sufficient strength when the rear surface of the projectile reaches it, the rear surface will be thoroughly shattered and dispersed. If not, large fragments of the rear portions of the projectile will survive and continue their flight unimpeded through the hole punched in the target by the front portions of the projectile.

In addition to the rarefaction due to the back face of the target, lateral expansion of the projectile is occuring which also generates rarefaction waves. The pressures in the shock are high enough to move the target material laterally, as is shown by the arrows moving upward into the target material. Behind the target, the material can expand laterally into a void, and so the expansion proceeds faster there. The region influenced by the lateral expansion can be identified by the velocities which have acquired an r-component of velocity.

The continuation of the process described is shown in Fig. 9, which pertains to the time of 4.2 μsec. Both rarefactions have eaten into the shocked region, reducing the pressures there. In spite of the pressure reduction which has occured at this point, it is interesting to note that the projectile, which was originally 10 cm in length, is at this time compressed into the region between $x = 5.3$ cm and $x = -1.6$ cm. The pressures in the shock, which is about to encounter the back of the projectile, range from about 2 megabars on the axis to about 0.2 megabars at the cylinder periphery. This is sufficient to thoroughly shatter the projectile.

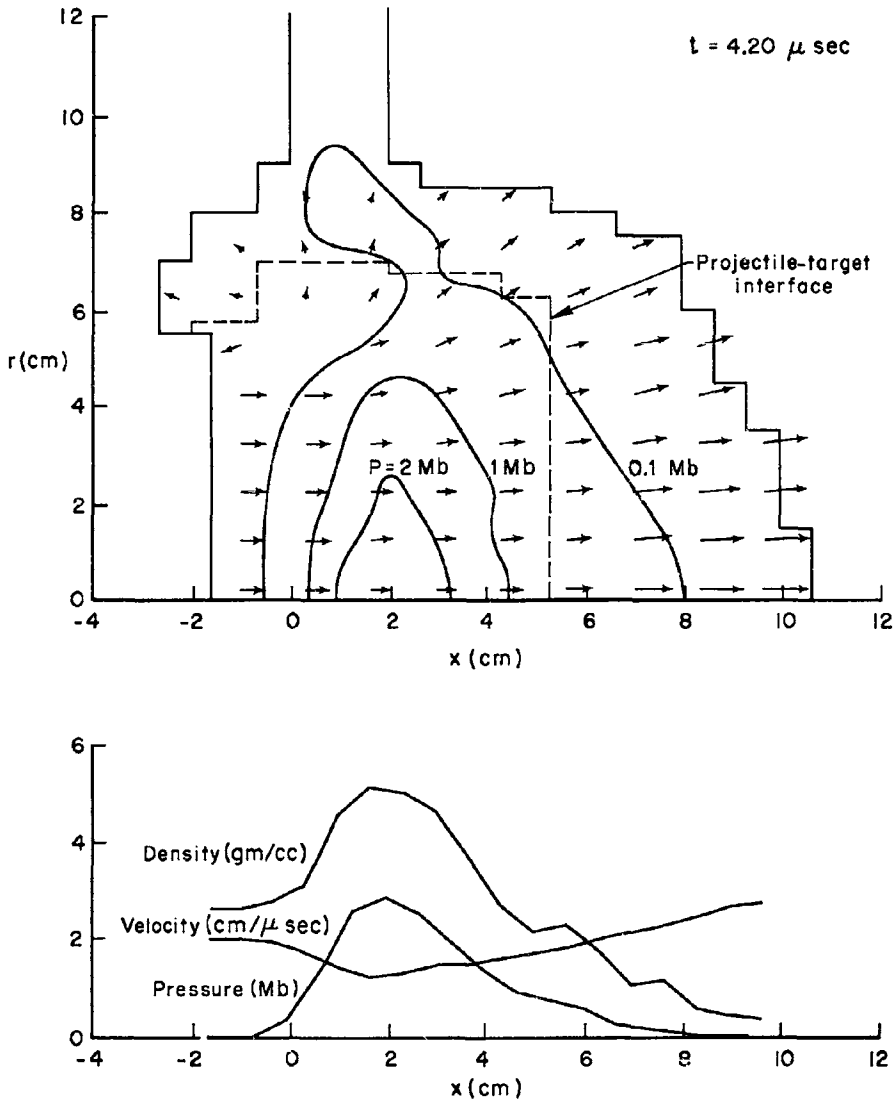

Fig. 9 —Aluminum cylinder (10-cm diameter, 10-cm length) striking 2-cm aluminum plate at 20 km/sec. Conditions: 4.20 μ sec after initial contact

The final stage of the process is shown in Fig. 10. At this time of 9.86 μsec, sufficient expansion of the material has occured to render all pressures zero. Density contours are plotted instead of pressure contours. On the model used in the calculation, the material is represented as a continuum, and the density is calculated on that basis. In reality, the material has undoubtedly broken up into particles at this time. The density reported may be expected to give quite accurately the density, averaged over particles and voids.

Unfortunately, there is no known method of estimating the particle sizes present in the diverging spray shown in Fig. 10. Were such an estimate possible, a complete description of the damage to be expected from this spray might be given. Available experimental evidence indicates that for a given projectile-target system the spray particles become smaller with increasing impact velocity. A qualitative discussion of the expected damage will be given later in this Memorandum.

One can see from Fig. 10 that the velocity field essentially radiates from a single point, the point being on the axis of symmetry at -8.8 cm. That is to say, if each velocity vector were projected backward to the axis of symmetry, it would intersect the axis at about -8.8 cm. One such constructed line is shown dashed in the figure. The flow is thus conical in nature, and further inspection shows that along a ray from the cone's apex, there is a positive velocity gradient, so that in flight the spray is elongating as well as expanding laterally. This implies that each particle will proceed with unchanged velocity from this time forward because there are no pressure forces and no material will accumulate in the future to create any, in view of the positive velocity gradient.

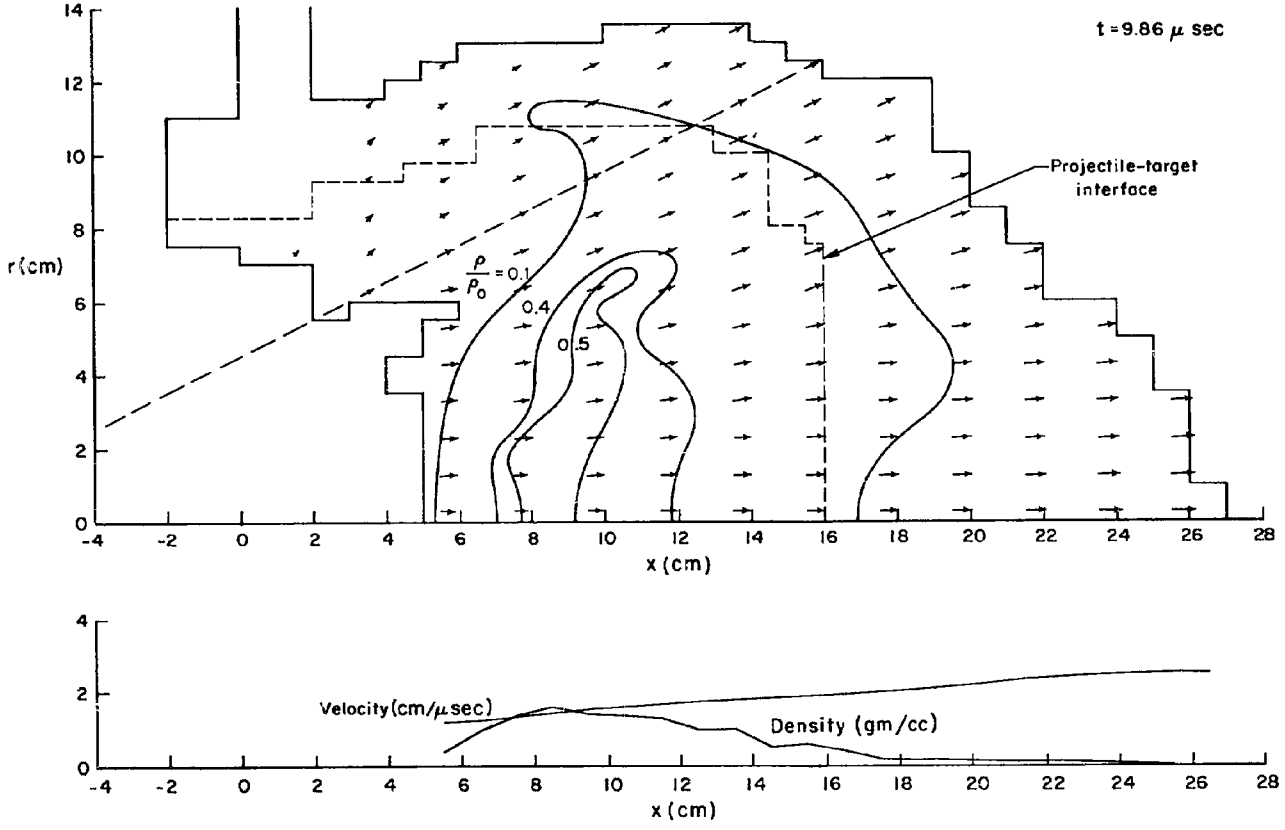

Fig. 10— Aluminum cylinder (10-cm diameter, 10-cm length) striking 2-cm aluminum plate at 20 km sec. Conditions: 9.86 μ sec after initial contact

Because of the conical nature of the flow, it is physically meaningful to prescribe the momentum per unit solid angle about the cone's apex. This quantity will remain fixed no matter how far the spray flies. One should note that this may be said only of a conical-type flow. In Fig. 11 the momentum per unit solid angle about the conical apex is shown as a function of angle from the axis of symmetry. To calculate these numbers, cones having 5-deg increments in apex half angle were laid out, and the momentum of material contained between them was summed. This momentum was then divided by the solid angle bounded by the two cones. The number thus obtained is plotted at the angle halfway between the two cones. The points are then connected by straight lines.

The results from both the 1- and 2-cm targets are shown, and the effect of target thickness is obvious. The spray from the thin target is more concentrated at the smaller angles, and the maximum dispersion angle is smaller. The physical reason for this will now be discussed.

In the series of Figs. 12 to 14, the impact of the same cylinder with a 1-cm target is presented. The qualitative features of the process are exactly the same. Quantitatively, a few differences appear. In Fig. 12, which pertains to a time of 2.75 μsec, it may be noticed that the left shock has been carried forward slightly. The reason for this is that the shock propagation velocity increases with shock strength, and the rarefaction from the rear of the target weakens the shock more quickly than in the case of the thicker target. For this reason, the shock will be weaker at corresponding times than the shock in the other case.

The lower pressures from this source lead to less lateral expansion.

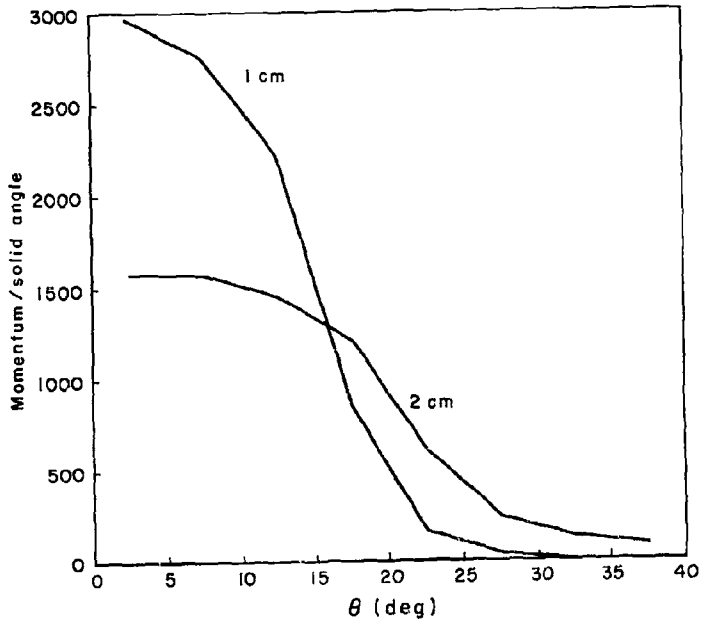

Fig. 11—Momentum per unit solid angle contained in the spray resulting from cylinder (length = diameter = 10 cm) striking aluminum plates of thickness 1 and 2 cm

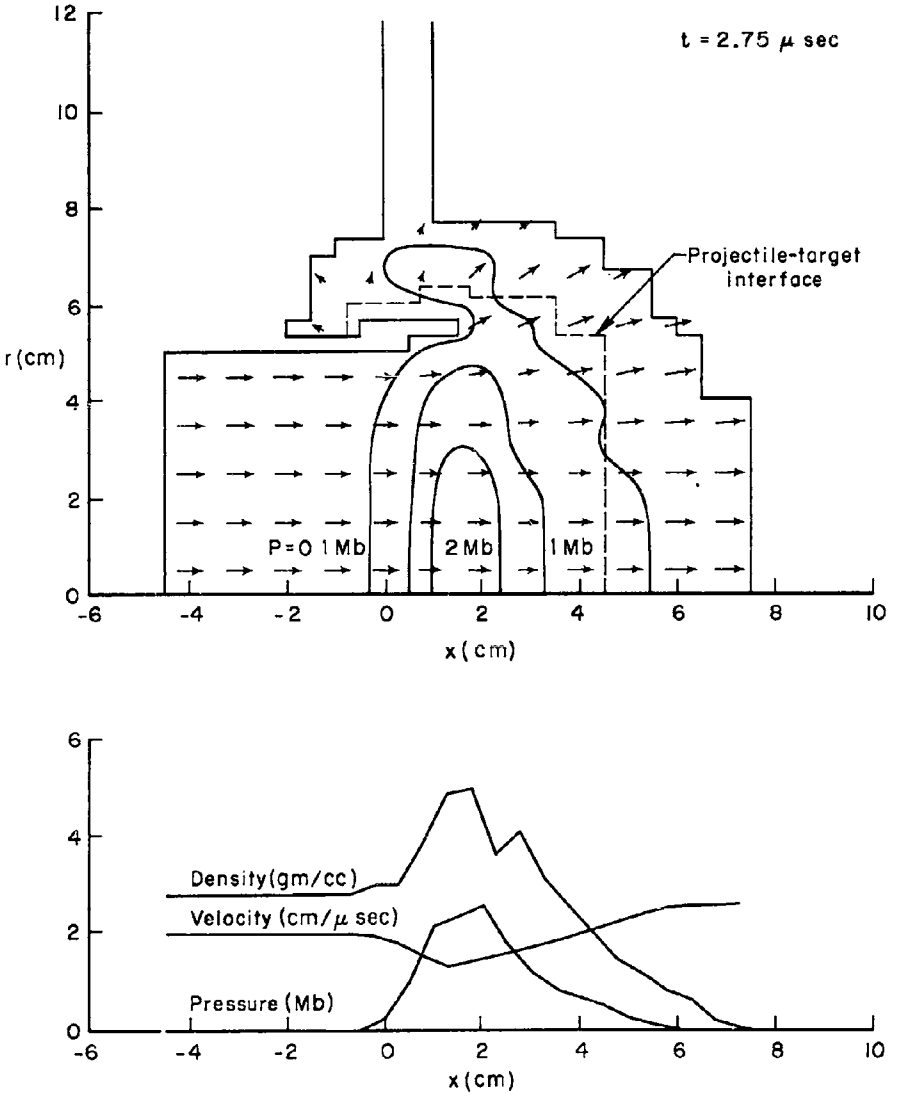

Fig. 12 — Aluminum cylinder (length = diameter = 10 cm) striking 1-cm aluminum plate. Conditions: 2.75 μ sec after initial contact

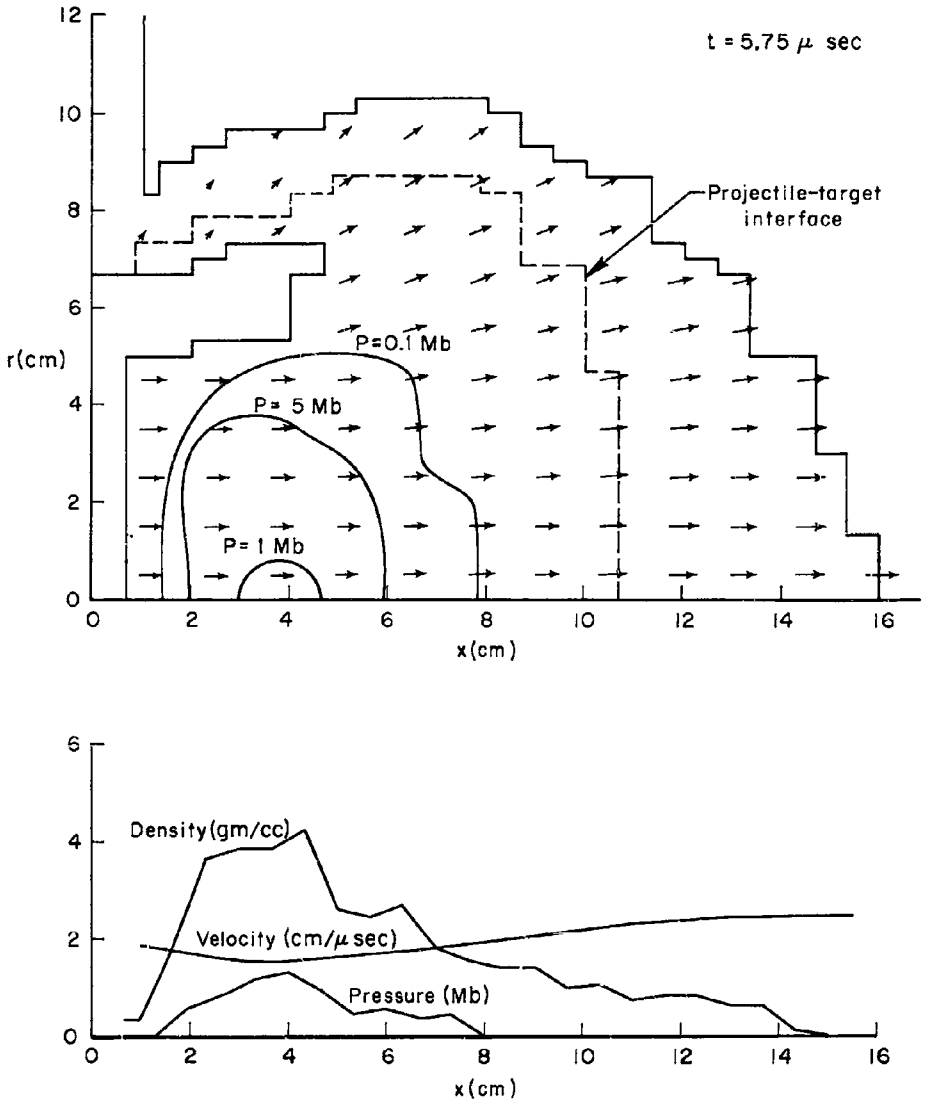

Fig. 13—Aluminum cylinder (10-cm diameter, 10-cm length) striking 1-cm aluminum plate at 20 km/sec. Conditions: 5.75 μ sec after initial contact

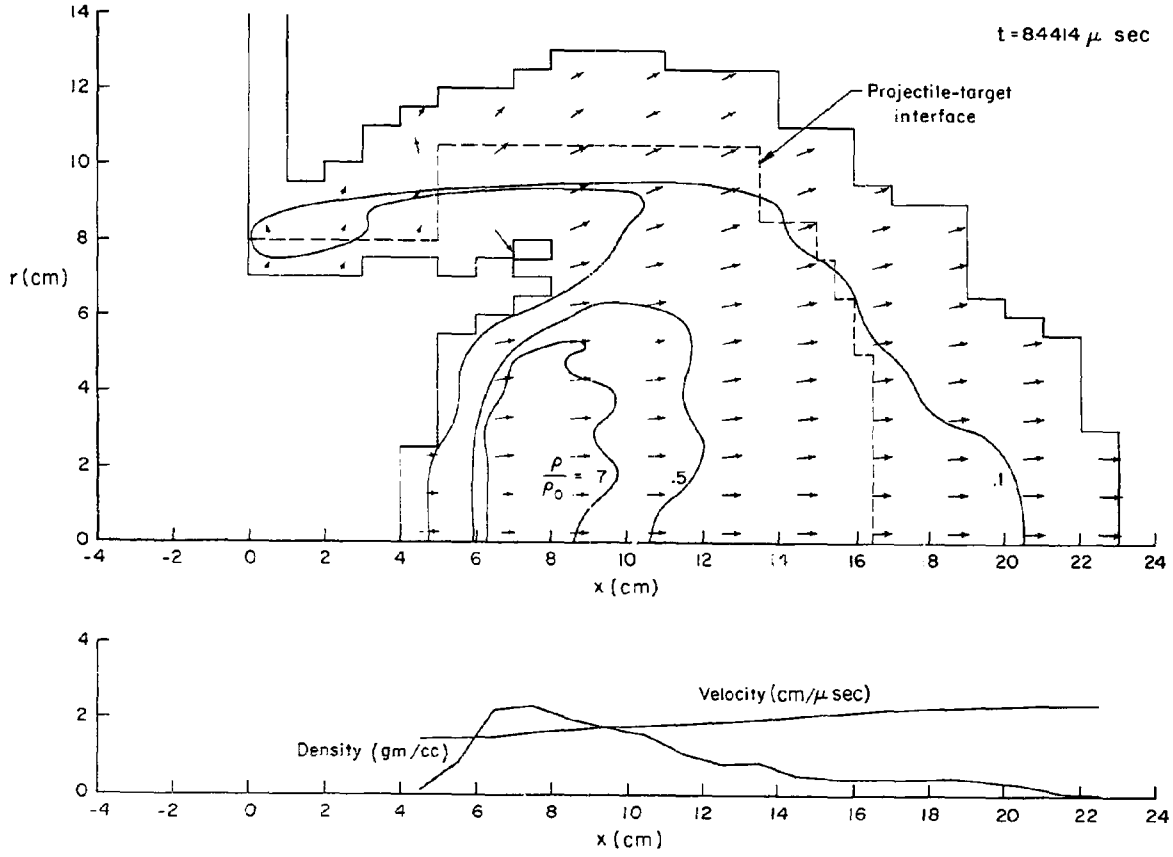

Fig. 14 — Aluminum cylinder (10-cm diameter, 10-cm length) striking 2-cm aluminum plate at 20 km/sec. Conditions: 8.44 μ sec after initial contact

This explains why more mass is carried in the forward direction and the maximum dispersion angle is smaller, as shown in Fig. 11.

For the same reason, the strength of the shock which reaches the rear projectile surface is also smaller, ranging from 1 megabar to somewhat less than 0.2 megabar in this case. These pressures should still be sufficient to thoroughly shatter the projectile.

Finally, a smaller hole will be produced in the thinner target, since less impulse per unit lateral area is applied to it, and the pressure in the thinner plate is more rapidly relieved by rarefaction waves. The final hole radius is estimated from these calculations to be about 9 cm for the thin target and about 12 cm for the thicker one.

It is clear from these considerations that the diameter of a hole created in a thin target will always be smaller than the crater diameter produced in a thick target. Figure 15 shows roughly how the hole diameter in a thin target will vary as a function of target thickness. The ordinate of the figure is D_h/d, where D_h is the hole diameter and d is the characteristic dimension of the projectile. The abscissa, t/d, is the target thickness in units of the projectile dimension. The figure indicates that in the limit of zero target thickness, the hole diameter approaches the projectile diameter, so that D_h/d approaches unity. As the target thickness is increased, the hole diameter increases rapidly until it reaches the limiting diameter, corresponding to the thick-target crater diameter. This limit is reached when the target thickness is of the order of the projectile dimension. After this point, the hole diameter on the entrance surface will remain essentially constant, but with further increase in target thickness a

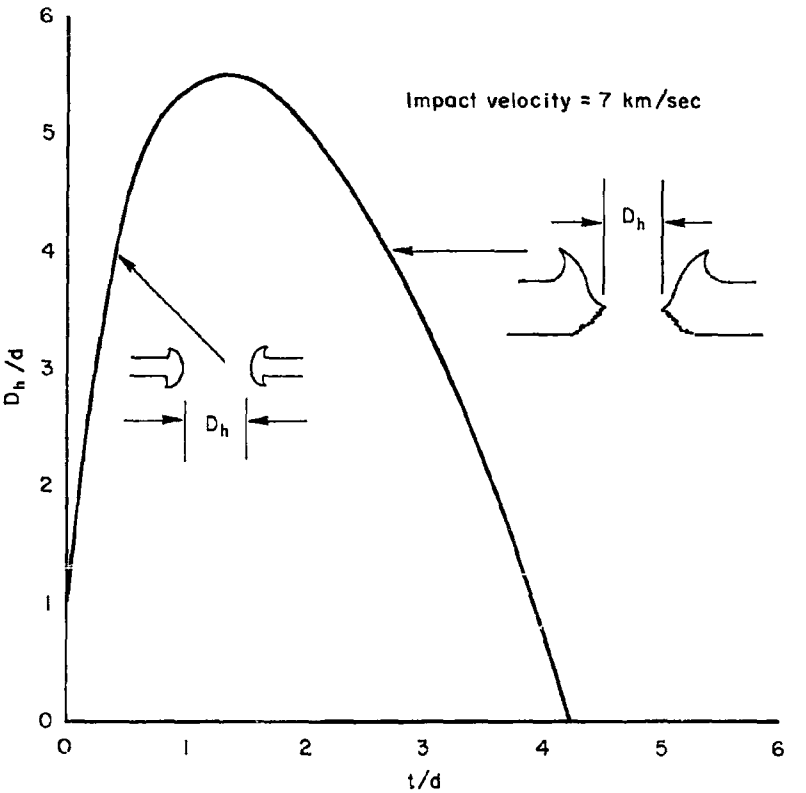

Fig. 15 — Expected hole diameter (D_h) at constant impact velocity as a function of target thickness (t) for 1100-F aluminum targets. Quantities are expressed in units of projectile dimension (d)

constriction will appear below the entrance surface. This is illustrated in the inset in Fig. 15. Below the constriction the hole enlarges due to spallation of the rear surface. The portion of the hole due to spallation will vary erratically from sample to sample and will also depend on such factors as the strength and brittleness of the sample. As the target thickness is further increased, the diameter of the constriction will decrease, finally becoming zero when the target attains a thickness of about three-quarters of the thick-target crater diameter. Figure 15 is sketched for the case of aluminum striking aluminum at 7 km/sec, a reasonable satellite orbital velocity. For this case, the thick-target penetration is about 2.75 projectile diameters. Therefore, the maximum hole diameter is about 5.5d, and the closure of the constriction occurs for a target thickness of about 4.1d.

The discussion of the physical process of thin-plate perforation has disclosed that such plates are amazingly efficient in shattering a hypervelocity projectile. Of course, the plate pays the penalty of having a hole blown in it during the process, and the hole dimensions have been discussed in the preceding section. We will now consider the damage which the spray of fine particles emerging from the rear surface may be expected to cause.

The damage will be a function of standoff--the separation between the back of the first plate and the next surface to be encountered. At small standoffs, the impact craters of the individual spray particles will overlap, with the result that a single rather deep crater would be produced in a thick target. In a thin target at small standoff, a clean perforation may be expected. The criterion for this type of

perforation is that a sufficiently high pressure be built up in the second target to occasion behavior of the hydrodynamic type. The shock, upon reaching the rear of the second plate, must blow it off and allow the momentum to proceed through in the manner just discussed for the first plate. If this occurs, almost all of the momentum passes through the second sheet, leaving only a clean perforation, and producing very little bulging or other distortion of the plate. At larger standoffs, the individual impact craters produced by the spray particles cease to overlap, and in a thick target, only the dimpling of the individual craters will be apparent. In a thin target, however, if the individual craters do not perforate the sheet, the momentum of the spray particle is entirely trapped within the plate. It may even be somewhat enhanced because of producing back splash. For such cases the behavior of the plate may be deduced by calculating the pressure pulse (pressure as a function of time and position) which acts upon it and solving the resulting problem in mechanics. The pressure is equal to the time rate of momentum arrival per unit area, a quantity which may be calculated from the theoretical data presented in Figs. 10 and 14.

Some general observations may be made on the nature of the pressure pulse received by the second plate. At any given angle, θ, the total momentum per unit area received by the second plate is a function of standoff, since it varies inversely as the square of the distance from the apex of the conical flow. Because of the velocity gradient along a given ray, the time required to impart this momentum will increase linearly with distance from the apex point. Thus, the peak pressure at any given angle may be expected to fall off inversely as the cube of the distance from the apex point.

At very great standoffs, the plate will withstand the effects of the pressure pulse very well, and the only damage expected is the pitting due to the individual fragments present in the spray. The depth of these pits will vary linearly with the dimension of the fragment which produces them. Therefore, an assessment of the damage from this source requires a knowledge of the fragment sizes present in the spray. As standoff is decreased, the pressure pulse will produce a bulge in the plate, whose severity increases with shorter standoff. The bulging deformation produces tension in the plate and stretches the material so that it thins out. At some critical standoff, the material in the bulge fails in tension, the failure originating at the crown. This failure is accompanied by cracks which propagate down the sides of the bulge as the sides flare out, forming large petals. The effects of standoff are very critical in this region, the bulge either remaining intact if no tensile failure occurs or petalling fully in the event of failure. The petalling failure usually produces much larger holes in the second plate than the primary projectile would produce in the absence of the first plate.

IV. SCALING LAW FOR DISSIMILAR-MATERIAL IMPACTS

A. E. Olshaker and the author have proposed a scaling law to predict the penetration resulting from an impact between a projectile and target of dissimilar materials.(1) Recent experimental data have verified the law for aluminum targets.

The form of the scaling law is

$$\frac{\pi_{B-A}(v)}{\pi_{A-A}(v)} = F_{BA}(v) \tag{4}$$

where π is the normalized penetration, p/d, and the subscript B-A denotes a projectile of material B striking a target of material A.

A simple extension of Eq. (4) is

$$\frac{\pi_{B-A}(v)}{\pi_{C-A}(v)} = \frac{F_{BA}(v)}{F_{CA}(v)} \tag{5}$$

The interpretation of Eq. (5) is this: If the penetration of any projectile material B into target material A is known at any impact velocity, then the penetration of any other projectile material C into target A at the same velocity may be predicted.

In Ref. 1, the normalized penetration ratios, $F_{BA}(v)$, are presented graphically for targets of eight common metals and one rock. For each target, projectiles of the same nine materials are considered.

The scaling law postulates that the normalized penetration ratio has the form

$$F_{BA}(v) = \frac{2u_{BA}(v)}{v}\left(\frac{\rho_B}{\rho_A}\right)^{1/3} \tag{6}$$

where ρ_B and ρ_A are the densities of projectile and target material, respectively. The quantity $u_{BA}(v)$ is the particle velocity produced behind the shock when a one-dimensional collision of material B on a stationary target of material A occurs at velocity v. It may be regarded as a measure of the mechanical coupling between the two materials in a hypervelocity impact. It is the velocity imparted to the target material by the projectile.

For impacts between similar materials

$$u_{AA}(v) \equiv \frac{v}{2} \tag{7}$$

leading to

$$F_{AA}(v) \equiv 1 \tag{8}$$

If the projectile material is stiffer* than the target material, then

$$u_{BA}(v) > \frac{v}{2} \tag{9}$$

and at the same impact velocity, projectile B generates larger velocities in the target than does projectile A. The densities correlate well with stiffness, so that in all cases treated it was found that stiffer projectiles led to $F_{BA}(v) > 1$. Conversely, soft projectiles generate smaller velocities in the target and lead to shallower craters.

*Stiffness is a measure of the shock pressure as a function of change in particle velocity across the shock. Stiffer materials have larger pressures for a given increment in particle velocity.

While scaling by means of the F-factors is regarded as most accurate, a rougher but more convenient scaling is also possible. An empirical fit to the results of F-scaling may be written in the form

$$\frac{\pi_{B-A}(v)}{\pi_{A-A}(v)} = \left(\frac{\rho_B}{\rho_A}\right)^{\beta_A(v) + 1/3} \qquad (10)$$

where $\beta_A(v)$ pertains to targets of material A. The functions, β_A, may all be presented on one graph, as in Fig. 16. In general, β-scaling agrees with the more accurate F-scaling to within 10 per cent. Calculation of the F-factors demands the knowledge of the shock Hugoniot of the projectile material at the impact velocities of interest. Where this information is not available, one may still use β-scaling to give a reasonable first estimate. The F-factors for aluminum targets are shown in Fig. 17.

In Fig. 18 the scaling law is tested against recent experimental data. All of the data in the figure pertain to 1100F aluminum targets. The data of Atkins, shown as circles in the figure, were obtained by firing saboted aluminum spheres. The data are presented unscaled in the figure, and good agreement with the author's theoretical results is obtained, as previously noted. The data of Liles and Goodman,[4] shown as triangles, pertain to saboted copper spheres impacting 1100-F aluminum. These data have been scaled down by the appropriate F-factor, shown in Fig. 17. If the scaling law is correct, the two sets of data should be brought to the same curve by this treatment. The scaling law gives remarkably exact agreement with the experimental data.

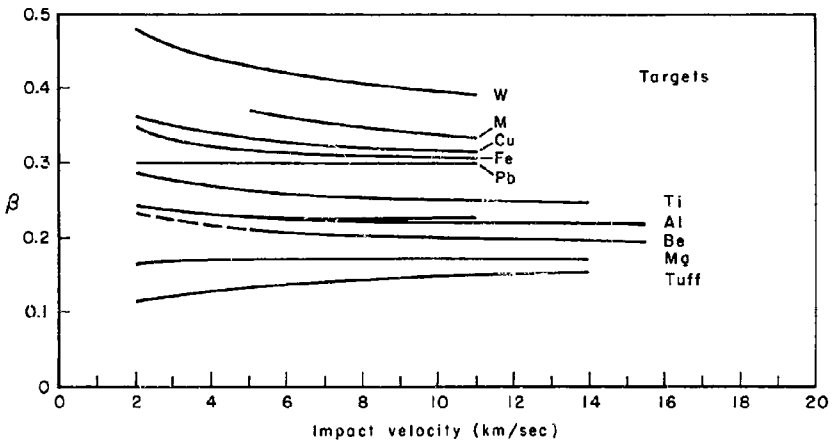

Fig. 16 — Values of β deduced from the normalized penetration–ratio curves

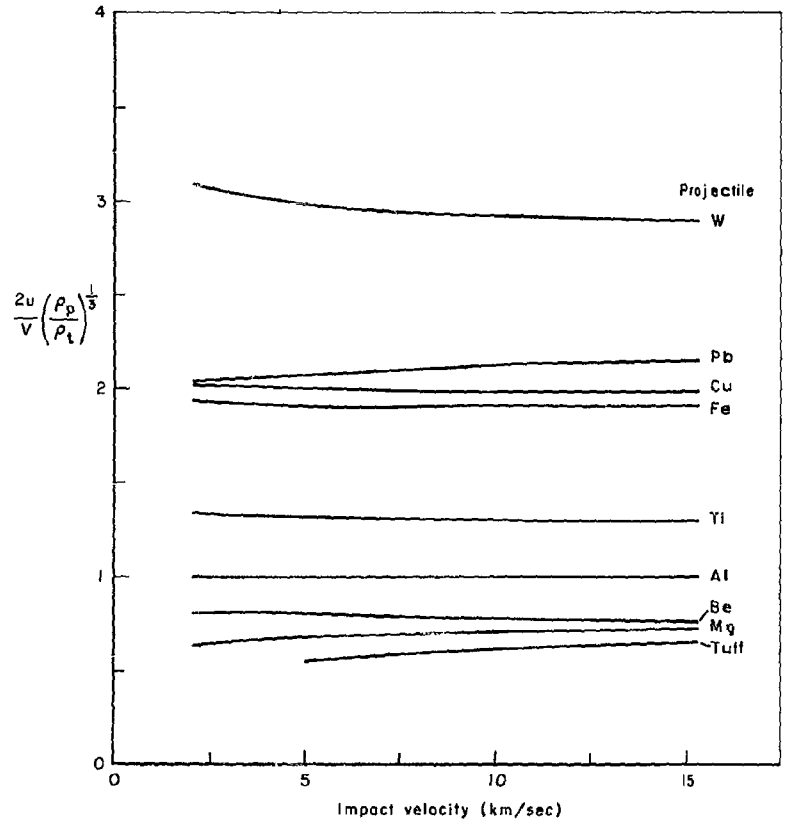

Fig. 17 — Normalized penetration ratios versus impact velocity for aluminum targets

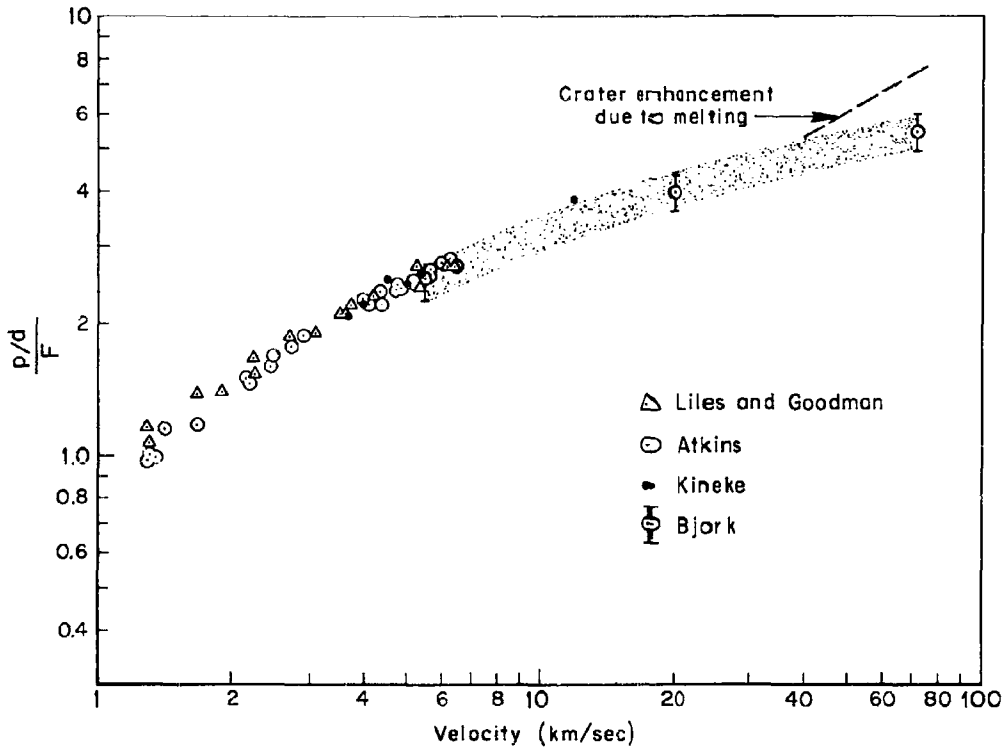

Fig. 18 — Dissimilar-material scaling law compared with experimental data for 1100-F aluminum targets. Aluminum projectile points (Atkins) shown unscaled. Copper projectile (Liles and Goodman) and steel projectile (Kineke) points reduced by factor given in Fig. 17

The preceding constitutes a well-controlled test of the scaling law, since the mass, geometry, and velocity of all the data were well known. In particular, there is an unambiguous characteristic dimension to use for the projectile, namely, the sphere diameter.

The data of Kineke are shown as the dark dots in Fig. 18. While the agreement is apparently good, more treatment was required before plotting. Kineke accelerates flat steel discs by explosive means. The characteristic dimension of these projectiles was taken to be the diameter of the equivalent sphere, that is, the steel sphere which has the same mass as his projectiles. It may be observed that such treatment brings his data into extremely good correspondence with the other two better-controlled sets. The agreement of his fastest point with the theoretical prediction of the author is encouraging.

In Fig. 19 the scaling law is tested for the case of 2024-T3 targets. The data have been treated in the same way, the aluminum projectile points being presented unscaled, and the other projectile points being scaled so as to bring them onto the aluminum curve. The data all lie below the theoretical prediction of the author, as discussed in the section on strength effects. There is more scatter at lower velocities for this target material, but the different data sets are coalescing satisfactorily at the higher velocities.

The shock Hugoniot data for the plastic projectiles are not available at the experimental velocities shown, so that β-scaling was required. At 7 to 10 km/sec, the data for plastic, aluminum, and steel projectiles--materials that span a large part of the projectile-material spectrum--are brought together satisfactorily.

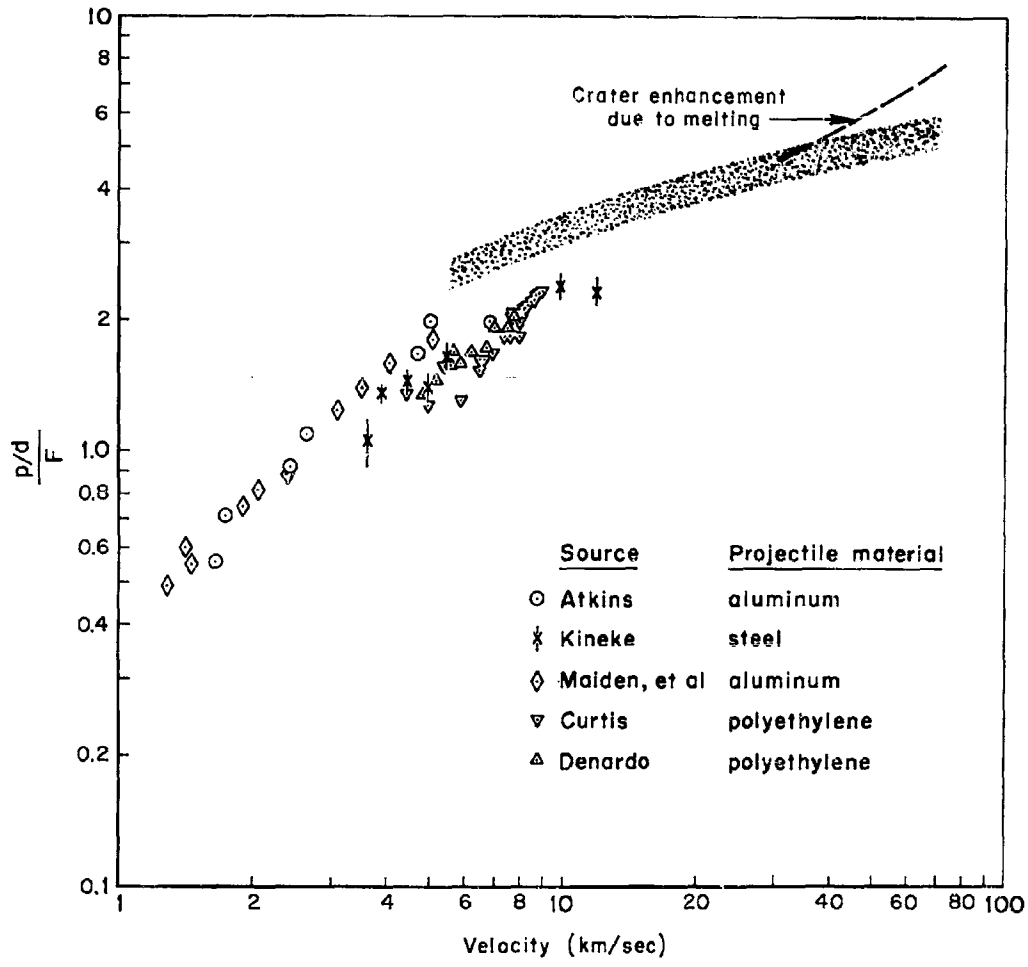

Fig. 19 — Dissimilar-material scaling law compared with experimental data for 2024-T3 targets.
Aluminum points are presented unscaled.
Steel points reduced by factor given in Fig. 17.
Polyethylene points increased by factor given in Fig. 16

It is believed that using the theoretical predictions of the author for aluminum-aluminum and iron-iron impacts and deriving the penetrations of other projectile materials in these targets by means of the scaling law just discussed will give an accurate estimate of any projectile penetration into these structural materials up to a velocity of 20 km/sec. Above that velocity, the possible effects of target melting must be taken into account.

REFERENCES

1. Bjork, R. L., and A. E. Olshaker, A Proposed Scaling Law for Hypervelocity Impacts Between a Projectile and a Target of Dissimilar Material, The RAND Corporation, RM-2926-PR (to be published).

2. Eichelberger, R. J., and J. W. Gehring, "Effects of Meteoroid Impacts on Space Vehicles," ARS J., Vol. 32, No. 10, October 1962, p. 1583.

3. Atkins, W. W., Proceedings of the Fourth Symposium on Hypervelocity Impact, Air Proving Ground Center, Air Research and Development Command, Eglin Air Force Base, Florida, September 1960.

4. Liles, C. D., and J. H. Goodman, Particle-Solid Impact Phenomena, Arnold Engineering Development Center, AEDC-TDR-62-202, November 1962.

5. Bjork, R. L., Effects of a Meteoroid Impact on Steel and Aluminum in Space, The RAND Corporation, P-1662, December 16, 1958.

6. Collins, R. D., Jr., and W. H. Kinard, The Dependency of Penetration on the Momentum Per Unit Area of the Impacting Projectile and the Resistance of Materials to Penetration, NASA TN D-238, May 1960.

7. Halperson, S. M., and W. W. Atkins, Proceedings of the Fifth Symposium on Hypervelocity Impact, Colorado School of Mines, Golden, Colorado (Host organization), November 1961.

8. Bjork, R. L., and A. E. Olshaker, The Role of Melting and Vaporization in Hypervelocity Impact, The RAND Corporation, RM-3490-PR (to be published).